

Instruction-Free Tuning of Large Vision Language Models for Medical Instruction Following

Myeongkyun Kang¹, Soopil Kim², Xiaoxiao Li³, and Sang Hyun Park¹,

Abstract—Large vision language models (LVLMs) have demonstrated impressive performance across a wide range of tasks. These capabilities largely stem from visual instruction tuning, which fine-tunes models on datasets consisting of curated image-instruction-output triplets. However, in the medical domain, constructing large-scale, high-quality instruction datasets is particularly challenging due to the need for specialized expert knowledge. To address this issue, we propose an instruction-free tuning approach that reduces reliance on handcrafted instructions, leveraging only image-description pairs for fine-tuning. Specifically, we introduce a momentum proxy instruction as a replacement for curated text instructions, which preserves the instruction-following capability of the pre-trained LVLM while promoting updates to parameters that remain valid during inference. Consequently, the fine-tuned LVLM can flexibly respond to domain-specific instructions, even though explicit instructions are absent during fine-tuning. Additionally, we incorporate a response shuffling strategy to mitigate the model’s over-reliance on previous words, facilitating more effective fine-tuning. Our approach achieves state-of-the-art accuracy on multiple-choice visual question answering tasks across SKINCON, WBCAtt, CBIS, and MIMIC-CXR datasets, significantly enhancing the fine-tuning efficiency of LVLMs in medical domains.

I. INTRODUCTION

Large vision language models (LVLMs) have demonstrated strong general-purpose capabilities across a wide range of visual language understanding and generation tasks [1]. This success is largely attributable to large-scale visual instruction tuning, where models are fine-tuned on datasets consisting of image-instruction-output triplets (Fig. 1(a)). Despite its effectiveness in enhancing adherence to diverse human instructions,

Corresponding author: Sang Hyun Park.

M. Kang is with the Department of Electrical and Computer Engineering, The University of British Columbia, Vancouver, BC V6T 1Z4, Canada, and also with the Department of Robotics and Mechatronics Engineering, Daegu Gyeongbuk Institute of Science and Technology (DGIST), Daegu 42988, Republic of Korea.

S. Kim is with the Division of Intelligent Robot, Daegu Gyeongbuk Institute of Science and Technology (DGIST), Daegu 42988, Republic of Korea.

X. Li is with the Department of Electrical and Computer Engineering, The University of British Columbia, Vancouver, BC V6T 1Z4, Canada, and also with the Vector Institute, Toronto, ON M5G 0C6, Canada.

S. H. Park is with the Department of Computer Science and Engineering, Pohang University of Science and Technology (POSTECH), Pohang 37673, Republic of Korea. (e-mail: sanghyunpark@postech.ac.kr)

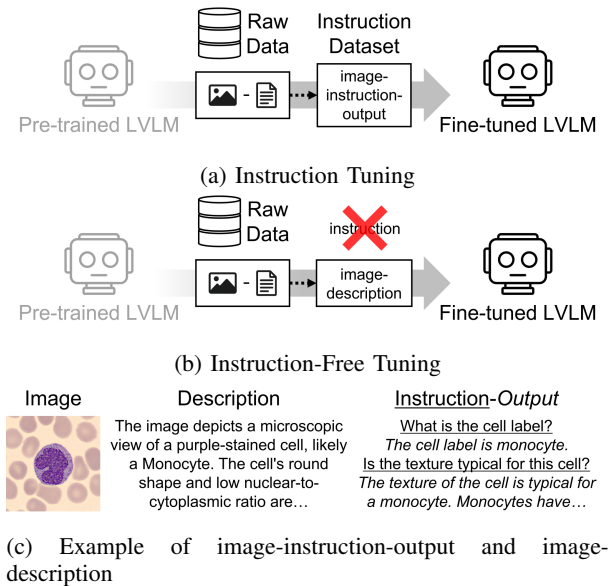


Fig. 1: Conceptual illustrations of (a) instruction tuning, which fine-tunes the model on curated instructions and outputs, and (b) instruction-free tuning, which fine-tunes the model solely on paired textual descriptions (e.g., radiology reports). Instruction tuning requires instruction-image-output triplets constructed by humans or LLMs prior to fine-tuning, whereas instruction-free tuning can be performed on image-description pairs without additional steps. Examples of an image, an instruction-output pair for instruction tuning, and a description used for instruction-free tuning are shown in (c).

visual instruction tuning is highly dependent on the scale and quality of the instruction dataset [2]. Therefore, instruction-tuned general-purpose LVLMs tend to perform poorly in domains with limited publicly available data, such as medicine.

Several studies have adapted LVLMs for medical applications by using instruction datasets specifically designed for the medical domain [3], [4]. Since medical images are typically paired with detailed textual descriptions (e.g., radiology reports or captions from PubMed Central), these studies leverage language-only large language models (LLMs) to transform image descriptions into conversational image-instruction-output triplets for visual instruction tuning. However, the frequent use of domain-specific abbreviations and terminology [5],

along with the need for expert-level contextual understanding [6], poses a significant challenge for constructing datasets using LLMs. Another challenge is that, radiology reports typically begin with a lesion description and conclude with a diagnostic impression [7], which leads to strong inter-sentence confounding dependencies within the constructed datasets. These characteristics lead to the overlooking of visual features and exacerbate hallucinations [8], thereby necessitating visual instruction tuning that accounts for these factors. Therefore, we revisit fine-tuning approaches that reduce reliance on handcrafted or generated instructions (as illustrated in Fig. 1(b)), aiming to avoid inefficiencies in constructing instruction datasets and to mitigate potential drawbacks caused by inadequate instructions.

Instruction-free tuning refers to fine-tuning LVLMS using only image-description pairs (e.g., radiology reports or captions), without relying on any instructions. To the best of our knowledge, this is the first work to formalize address this task for instruction-tuned LVLMS. However, fine-tuning a model without human-curated instructions introduces additional challenges, particularly when it leverages on the inherent properties of paired raw data as text instructions (e.g., “Describe this medical scan”) [4]. Paired descriptions (e.g., radiology reports or captions) do not perfectly align with the natural response (e.g., “The image...”) that would typically follow a conversational instruction (e.g., “Describe...”). The misalignment between the instruction-description pairs in the fine-tuning and pre-training datasets poses a risk of degrading the instruction-following capability of the pre-trained LVLMS.

Specifically, this may lead to *image-dependence*, where the model loses its pre-trained instruction-following capability and generates fixed-style responses that rely excessively on the image regardless of the given instruction (see Fig. 7). For instance, a model fine-tuned for report generation may fail to respond to other types of queries (e.g., “Is the texture typical...”) and struggle to generalize to question-answering tasks beyond report writing. Additionally, this may result in *instruction-dependence* (or *parameter-dependence*), where the model responds appropriately only to instructions encountered during fine-tuning and fails to generate responses aligned with the fine-tuning data for unseen instructions (instead respond based on the pre-trained knowledge; see other LVLMS in Table I). Furthermore, due to the nature of instruction-following LVLMS, instructions seen during fine-tuning are not guaranteed to be provided at inference time, highlighting the importance of preventing overfitting to such instructions.

In response to these challenges, we introduce a *proxy instruction* that is optimized to align with the set of image-description pairs in the fine-tuning dataset. Unlike conventional fine-tuning, which uses text instructions and optimizes model parameters, our method jointly updates both learnable proxy instructions and model parameters. This enables the LVLMS to adapt to domain-specific datasets without degrading its instruction-following capability through a well-aligned instruction. As a result, the fine-tuned model can flexibly respond to a wide range of text instructions in the medical context during inference. Furthermore, we refined the proxy instruction through an exponential moving average, i.e., a

momentum proxy instruction. This mitigates overfitting to a specific proxy instruction and allows the remaining parameters to leverage compensated representations that reflect overall fine-tuning trends.

In addition, diagnostic conclusions can often be inferred from the preceding text alone (e.g., findings), leading models to overlook visual features when generating the later part of the response. In this context, we propose a strategy, *response shuffling*, which randomly shuffles the sentence order of the ground truth description, thereby preventing the model from relying too heavily on previous words. Notably, employing a proxy instruction disregards the negative effects of shuffling output order during fine-tuning, enabling a simple strategy to substantially enhance medical visual question answering (VQA) performance.

In summary, the contributions of this paper are as follows:

- We introduce and formalize *instruction-free tuning*, a novel paradigm for fine-tuning LVLMS that eliminates the need for handcrafted or generated instructions, addressing a key bottleneck in adapting models to medical domains.
- We propose a *momentum proxy instruction* designed to preserve the instruction-following capability of the pre-trained LVLMS during fine-tuning, while promoting updates for parameters that remain valid during inference. Additionally, we propose a *response shuffling* strategy to mitigate the model’s over-reliance on previous words, facilitating more effective fine-tuning of medical LVLMS.
- We demonstrate that our fine-tuned model achieves state-of-the-art accuracy in multiple-choice VQA evaluations on the SKINCON, WBCAtt, CBIS, and MIMIC-CXR datasets.

II. RELATED WORKS

A. Instruction Tuning

Instruction tuning fine-tunes a model using a dataset consisting of instruction-input-output triplets. In particular, the instruction specifies the task (i.e., a question), the input provides supplementary context (e.g., an image), and the output is the expected response based on the instruction and input. As one of the early studies, Natural Instructions [9] fine-tuned a model with an instruction dataset constructed by integrating 61 datasets. Recently, an alternative approach that constructs instruction datasets using LLMs was proposed; Alpaca [10] efficiently fine-tuned the LLaMA [11] using 52K instruction-output pairs generated by an instruction-tuned GPT-3.5 [12]. Moreover, Self-Instruct [13] proposed a method for enabling an LLM to follow diverse instructions by iteratively generating and fine-tuning on synthetic instruction-output data with minimal human intervention. However, applying these methods to visual data is challenging because image generation in pixel space is inherently more difficult than text generation. Therefore, prior work has focused on constructing instruction datasets from paired image-text data (e.g., LLaVA [14]), rather than relying on synthetic data generation. Moreover, these methods are less effective at improving the performance of fine-tuned models when LLMs possess limited domain-specific knowledge.

B. Visual Instruction Tuning

Building on the success of instruction tuning, visual instruction tuning with LLMs was introduced for vision tasks. LLaVA [14] integrated CLIP’s vision encoder [15] with LLaMA [11], and was fine-tuned on an instruction dataset generated by language-only GPT-4 [12]. Recently, LLaMA-3.2-Vision [16] extended LLaMA 3.1 by adapting cross-attention layers to integrate the image modality with language. Additionally, alternative LLMs have been integrated into the vision domain, such as Qwen2.5-VL [17], which utilizes patch grouping and window attention to efficiently process large numbers of visual tokens.

These successes in LVLMs extended to medical domains. LLaVA-Med [1] was fine-tuned on an instruction dataset generated by GPT-4 [12], based on biomedical image-caption pairs from PubMed Central (PMC). Recently, PubMedVision [4] and MedGemma [3] have been fine-tuned on carefully curated medical datasets from PMC and other publicly available sources, significantly enhancing their medical capabilities. One study [18] attempted instruction-free tuning by using language-only instruction-output pairs and image-caption pairs with a fixed set of instructions. However, none of the existing methods completely avoided employing text instructions during LVLM fine-tuning. To our knowledge, this is the first approach to enable fine-tuning of instruction-tuned LVLMs without using any text instructions.

III. METHOD

A. Overview

Our framework is illustrated in Fig. 2. It comprises a vision encoder g (a vision transformer [19] followed by projection layers) and a language model f . Given an image X_v , a prompt X_p containing an instruction (e.g., a question), and the ground truth output y (e.g., an answer or description), the image X_v is fed into g to extract key-value matrices KV_v for generating responses conditioned on the image and the instruction. Specifically, f employs a cross-attention layer [16], [20] to integrate the query matrix derived from X_p with KV_v to generate the response \hat{y} . During fine-tuning, we compute an autoregressive loss L between y and \hat{y} to update the vision encoder g , while keeping the parameters of f frozen, following [21]. The following section provides details of supervised fine-tuning for *instruction tuning* and *instruction-free tuning*.

B. Instruction Tuning

We start by formulating *instruction tuning*. Instruction tuning fine-tunes the model on an image X_v , a prompt X_p containing a text instruction (i.e., a question), and a ground-truth output y (i.e., an answer). Formally, supervised fine-tuning for instruction tuning is defined as follows:

$$L(g) = - \sum_{i \in \mathcal{I}_Y} \log f(y_i | X_v, X_p, y_{<i}; g), \quad (1)$$

where \mathcal{I}_Y denotes the set of indices corresponding to the output sequence y , and $y_{<i}$ represents all previously generated tokens. However, constructing high-quality instruction

datasets consisting of carefully curated instruction-output pairs corresponding to medical images is challenging and often incurs substantial costs. As a result, prior studies [1], [4] leverage inherent properties of medical data as text instructions (e.g., “Describe this medical scan”) to construct instruction datasets. In practice, paired descriptions (e.g., radiology reports) do not perfectly align with the natural conversational responses expected from text instructions. This misalignment between instruction-description pairs in fine-tuning and pre-training datasets risks degrading the instruction-following capability of pre-trained LVLMs. Additionally, this may lead to either (a) *image-dependence*, in which the model generates fixed-style responses regardless of the instruction, or (b) *instruction-dependence*, where the model performs well only for instructions identical to those seen during fine-tuning. To address these issues, we introduce *instruction-free tuning*, which reduces reliance on curated instructions by employing only image-description pairs during fine-tuning.

C. Instruction-Free Tuning

In instruction-free tuning, the model is fine-tuned using an image X_v , a prompt X_p containing a *proxy instruction*, and a ground-truth description y . Unlike instruction tuning, which requires curated text instructions during fine-tuning, our approach employs a proxy instruction that is optimized to align with image-description pairs. The well-aligned proxy instruction enables an LVLM to adapt to domain-specific datasets without degrading its pre-trained instruction-following capability. Next, we present the details of instruction-free tuning with the proxy instruction.

1) *Proxy Instruction*: Let the proxy instruction $t = \{t_1, \dots, t_N\}$ be defined as a set of N continuous vectors, each with the same dimensionality as the word embeddings. The proxy instruction replaces the text instruction (e.g., a question) in the prompt X_p with learnable vectors during fine-tuning, in order to preserve the LVLM’s pre-trained instruction-following capability. Given the nature of instruction-following LVLMs, where instructions seen during fine-tuning are not guaranteed to be provided at inference time, we design a proxy instruction as a substitute for text instructions during fine-tuning and discard it at inference time. During fine-tuning, we feed a prompt X_p containing the proxy instruction t into f . Since f is differentiable, gradients can be propagated to update t , enabling the model to derive an well-aligned instruction from the dataset. To optimize t , we compute an autoregressive loss L between y and \hat{y} , as defined in Eq. 1, with the inclusion of t . Formally, supervised fine-tuning for instruction-free tuning is defined as:

$$L(g, t) = - \sum_{i \in \mathcal{I}_Y} \log f(y_i | X_v, X_p, y_{<i}; g, t). \quad (2)$$

For simplicity, supplementary tokens in X_p , such as `<|eot_id|>`, are omitted. The proxy instruction is optimized to align with image-description pairs, thereby mitigating the negative impact on the pre-trained instruction-following capability of LVLMs during fine-tuning. This approach is particularly suitable for medical domains, since it is infeasible

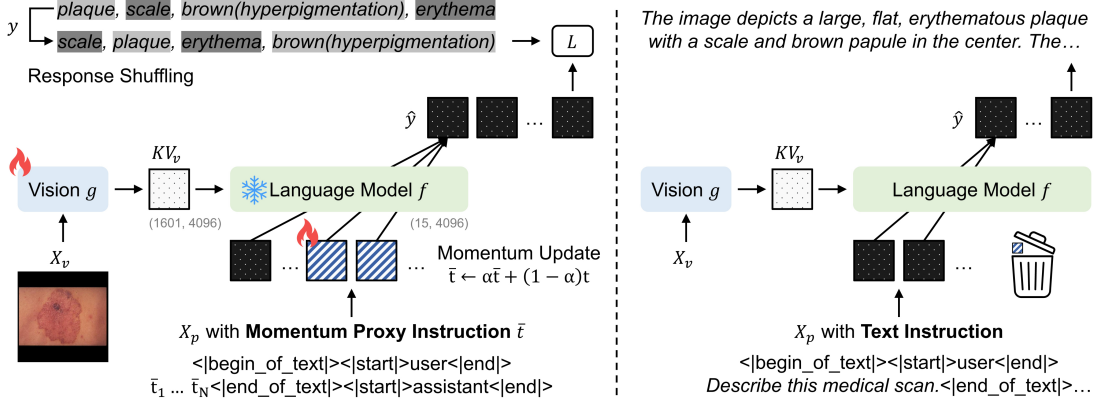


Fig. 2: An illustration of our instruction-free tuning framework. The vision encoder g extracts key-value matrices KV_v from an image X_v , which are then integrated into a prompt X_p for the language model f to generate the response \hat{y} . For instruction-free tuning, the text instruction in X_p is replaced with the momentum proxy instruction \bar{t} . During supervised fine-tuning, g is updated with autoregressive loss L between the response \hat{y} and the ground truth y . In parallel, (warm-up initialized) \bar{t} is gradually updated via exponential moving average of the proxy instruction t . During inference, \bar{t} is discarded, and a conversational text instruction (e.g., “Describe...”) is used to generate a natural language response (e.g., “The image depicts...”).

to fully provide all possible instructions during fine-tuning, and overfitting to such instructions results in the aforementioned *image-dependence* and *instruction-dependence*. Notably, the proxy instruction differs from that used in Prefix-Tuning [22]. In Prefix-Tuning, the learnable vectors are used during inference, whereas in our method they serve as a proxy during fine-tuning and are discarded at inference.

2) *Momentum Proxy Instruction*: Although the optimized instruction t is well aligned with its corresponding descriptions, t is replaced with a conversational text instruction at inference. This can lead to overfitting and over-reliance on proxy instructions, thereby degrading the inference performance of a fine-tuned LVLM. To mitigate this issue, we aim not to directly update the proxy instruction via gradient descent during fine-tuning. One possible alternative is to obtain a proxy instruction in a prior stage and fix it during subsequent training; however, this approach fails to capture the overall fine-tuning trends of the remaining learnable parameters. Instead, we refine the proxy instruction using an exponential moving average to capture overall fine-tuning trends [23], which promotes parameter updates to the vision encoder g and reduces sensitivity to t during generation. Formally, we update the momentum proxy instruction \bar{t} as follows:

$$\bar{t} \leftarrow \alpha \bar{t} + (1 - \alpha)t, \quad (3)$$

where $\alpha \in [0, 1)$ denotes the momentum coefficient. The parameters g are updated immediately via Eq. 2, whereas \bar{t} evolves gradually. Although \bar{t} is not directly updated via gradient descent, this design leads to more stable optimization by capturing the overall fine-tuning trends of the remaining parameters. The overall instruction-free tuning procedure with the momentum proxy instruction is summarized in Algorithm 1. Notably, to improve efficiency, we first optimize t while keeping g frozen as a warm-up stage, and then use the fine-tuned t to initialize \bar{t} , rather than using random initialization.

Algorithm 1 Instruction-free tuning process.

- 1: **Input:** Vision encoder g , language model f , ground truth description y , learning rate η , momentum coefficient α
 - 2: $t \leftarrow \mathcal{N}(0, \sigma^2)$
 - 3: **while** not warmed-up **do**
 - 4: $y \leftarrow \text{RS}(y)$ // Response Shuffling. See Eq.4
 - 5: **Compute** $\mathcal{L} \leftarrow L(g, t)$ // See Eq.2
 - 6: $t \leftarrow t - \eta \nabla_t \mathcal{L}$
 - 7: **end while**
 - 8: $\bar{t} \leftarrow t$
 - 9: **while** not converged **do**
 - 10: $\bar{t} \leftarrow \alpha \bar{t} + (1 - \alpha)t$
 - 11: $y \leftarrow \text{RS}(y)$
 - 12: **Compute** $\mathcal{L} \leftarrow L(g, \bar{t})$
 - 13: $g \leftarrow g - \eta \nabla_g \mathcal{L}$; $t \leftarrow \bar{t} - \eta \nabla_{\bar{t}} \mathcal{L}$
 - 14: **end while**
-

D. Response Shuffling

In medical domains, the past activations ($y_{<i>i</i>}$) of X_v are likely to be largely overlooked during supervised fine-tuning. Specifically, radiology reports typically begin with lesion descriptions and conclude with diagnostic impressions, causing the model to over-rely on previously predicted tokens and overlook visual inputs. To address this issue, we randomly shuffle y during fine-tuning to prevent the model from relying on previous tokens when generating responses. Formally,

$$\text{RS}(y) = \text{Join}(\text{Shuffle}(\text{Split}(y))), \quad (4)$$

where `Split` segments y by a separator (e.g., “;”), `Shuffle` randomly permutes the segments, and `Join` reconstructs the permuted y using the original separator. Notably, the goal of our fine-tuning is not to train the model to generate high-quality radiology reports, but rather to adapt the model to a domain-specific dataset while preserving the pre-trained instruction-following capability. Therefore, the negative effects of shuffling the output order during fine-tuning are disregarded (see Fig. 7).

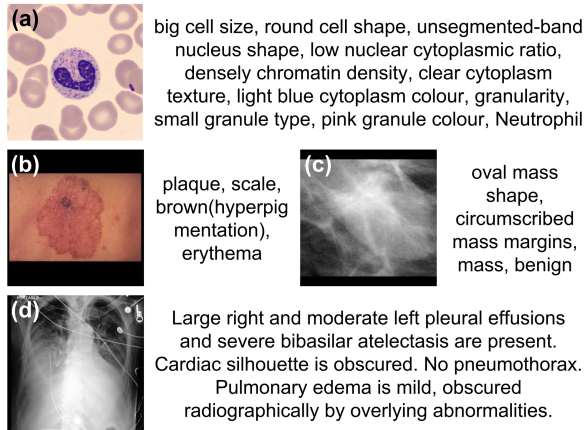


Fig. 3: Examples of the medical report for the (a) SKINCON, (b) WBCAtt, (c) CBIS, and (d) MIMIC-CXR datasets.

IV. EXPERIMENTS

A. Datasets

We conducted experiments on four richly annotated medical datasets, as shown in the Fig. 3.

- **SKINCON** [24] is a dermatology dataset that contains 3230 images from the Fitzpatrick17k [25]. Each image was manually annotated by dermatologists using 48 clinical attributes, such as *plaque*. The dataset was split into 80% for training, 10% for validation, and 10% for testing.
- **WBCAtt** [26] is a dataset consisting of 10298 microscopic images of white blood cells, such as *neutrophils*. Each image was annotated with 11 attributes, such as *cell size*, based on guidelines defined by pathologists. The dataset was split into 6179 images for training, 1030 for validation, and 3099 for testing.
- **CBIS** [27] is a digitized mammography dataset consisting of 892 mass cases and 753 calcification cases. Each mammogram was annotated with *pathology*, *abnormality types*, and BI-RADS descriptors (e.g., *mass shape*). This dataset provides cropped images of lesions extracted through ROI segmentation. For our experiments, we used cropped images along with their corresponding attribute annotations. The dataset was split into 90% for training and 10% for validation, and the official test split was used for testing.
- **MIMIC-CXR** [28] is a chest X-ray dataset that contains 377110 images corresponding to 227835 radiographic studies. Each study is paired with a free-text radiology report obtained from the Beth Israel Deaconess Medical Center’s electronic health record system for the period 2011-2016, and we used version 2.1.0 for our experiments. To extract image-relevant content from free-text reports, we used the findings and impression sections of LLM-annotated MIMIC-CXR reports from [29]. To select frontal chest X-rays, we employed CheXmask [30] to filter out non-chest X-ray images with a Reverse Classification Accuracy (RCA) below 0.7.

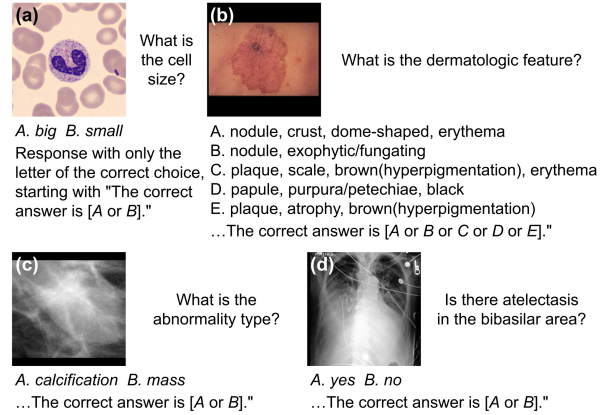


Fig. 4: Examples of multiple-choice VQA for the (a) SKINCON, (b) WBCAtt, (c) CBIS, and (d) MIMIC-CXR datasets.

B. Data Preparation for Instruction-Free Evaluation

To evaluate the fine-tuned LVLMs in instruction-free tuning scenarios, we converted the training split data into a medical report (see Fig. 3), while the validation and test split data into a multiple-choice VQA (see Fig. 4). When converting to medical reports, attribute annotations were formatted into plain text. In the **SKINCON** dataset, a medical report was formatted by listing the names of the items marked as *present* among the 48 attributes, such as “*plaque, scale*.” In the **WBCAtt** dataset, a medical report was formatted by listing 8 attributes in the form of $\{value\} \{name\}$ (e.g., “*big cell size*”). Meanwhile, yes/no attributes, such as *granularity*, were added using the $\{name\}$ when present, whereas *label* attributes were added using the $\{value\}$. In the **CBIS** dataset, a medical report was formatted by listing the $\{value\}$ of *abnormality* and *pathology* attributes. The remaining attributes were added in the form of $\{value\} \{name\}$. For the **MIMIC-CXR** dataset, the preprocessed reports from [29] were used without further processing.

When converting to multiple-choice VQA, attribute annotations were formatted into question-answer pairs, usually with five options. The question was constructed using the attribute name in the form “*What is the {name}?*”, whereas for the SKINCON dataset, the fixed question “*What is the dermatologic feature?*” was used. For multiple-choice options, the annotated attribute value was set as the correct answer, while randomly sampled non-overlapping values from the same attribute served as the incorrect options. Attributes with fewer than five options (e.g., yes/no) were converted into a limited choice set (e.g., two options). For **MIMIC-CXR** evaluation, we used the Medical-CXR-VQA dataset [31]. This dataset consists of VQA pairs for chest X-ray interpretation built from the MIMIC-CXR dataset, covering questions on abnormalities, presence, view, location, level, and type. Since we used only frontal chest X-rays for our experiments, we excluded view-related question types. For consistency with the other datasets, we added incorrect options to convert the dataset into a multiple-choice VQA format with five options. Incorrect options were set to different values within the same question type, while yes/no questions were limited to two

options. For abnormality-type questions with multiple disease answers, we conducted VQA separately for each disease, setting each abnormality as a separate correct choice. To promote reproducibility and fair comparison, we release the full instruction-free tuning benchmark for the SKINCON, WBCAtt, and CBIS datasets, including the preprocessing pipelines for the medical reports and the multiple-choice VQA evaluation protocols.

C. Implementation Details

The proposed method was developed on top of LLaMA-3.2-11B-Vision-Instruct [16], and fine-tuning was performed using the torchtune framework [21]. For models with proxy instructions, the number of instruction vectors N was set to 8, and the momentum coefficient α was set to 0.999. The warm-up stage was conducted for one epoch (approximately 3000 steps), while the fine-tuning stage was conducted for five epochs. We mainly followed the default settings in torchtune for supervised fine-tuning, such as a batch size of 2 and the AdamW optimizer. We use an input resolution of 560×560 for fine-tuning and evaluation. For all datasets, we specified the response style at the end of each question (e.g., “*Response with...*”; see Fig. 4) and extracted the predicted choice (e.g., A) by parsing the model’s output. We evaluated multiple-choice VQA using accuracy by comparing the selected choices with the correct answers. We conducted each experiment three times with different random seeds for the main results and report the average accuracy. As demographic annotations were not consistently available across all datasets, these variables were not incorporated into the analysis.

V. RESULTS

A. Multiple-choice VQA

1) *Main Results*: We first compared our method against other LVLMS without fine-tuning (*w/o* FT) on the SKINCON, WBCAtt, and CBIS datasets, including general LVLMS such as LLaMA-3.2-11B-Vision-Instruct [16] and Qwen2.5-VL-3B-Instruct [17], as well as medical LVLMS such as PubMedVision-7B-Qwen2.5VL [4] and MedGemma-4B-it [3]. We then compared our method with fine-tuned (FT) LLaMA-3.2-11B-Vision, Qwen2.5-VL-3B, and MedGemma-4B using a text instruction (i.e., “*Describe this medical scan*”). Fine-tuning of Qwen2.5-VL-3B and MedGemma-4B followed the settings described in their original papers. Additionally, we compared our method with BLIP-2 [32], which is trained on image-text pairs and is capable of performing VQA tasks. Note that the language model in BLIP-2 is not instruction-tuned and thus has limited instruction-following ability compared to the other LVLMS in our comparison. We refer our method as **InstFree**, which fine-tuned the model using the momentum proxy instruction, while **InstFree w/ RS** fine-tuned it with both the momentum proxy instruction and response shuffling. Since the WBCAtt and CBIS datasets provided attribute names, we reported the accuracy for each attribute separately.

Table I shows the multiple-choice VQA accuracy on the SKINCON, WBCAtt, and CBIS datasets. The accuracy of models without fine-tuning (*w/o* FT) is consistently lower than

that of fine-tuned models. Notably, MedGemma-4B underperforms compared to non-medical LVLMS, which we attribute to its primary fine-tuning on specific types of medical data, such as pathology and chest X-rays, suggesting that recent medical LVLMS may face challenges in generalizing across all types of medical data. Overall, these results highlight that fine-tuning LVLMS is crucial for downstream tasks in the medical domain, as it yields substantial performance improvements.

Although LLaMA-3.2-11B-Vision (FT) achieves comparable accuracy on the CBIS dataset, its average accuracy across all three datasets is lower than that of the proposed method, highlighting the limitations of naively incorporating a text instruction during fine-tuning. In contrast, the accuracies of Qwen2.5-VL-3B (FT) and MedGemma-4B (FT) are significantly lower than that of LLaMA-3.2-11B-Vision (FT). This discrepancy is not due to the limited model capacity of Qwen2.5-VL-3B and MedGemma-4B, but rather to their strong dependence on instructions, i.e., *instruction-dependence*. Specifically, the fine-tuned model generates correct responses to certain instructions (i.e., “*Describe this medical scan*”), but fails to respond appropriately to other types of instructions, such as “*What is the cell shape?*”, instead responding based on its inherent pre-trained knowledge [33]. Notably, even though MedGemma-4B has been fine-tuned, it still shows low accuracy on the SKINCON dataset. This is likely due to the absence of explicit attribute names in the medical reports and the limited instruction-following capability of the pre-trained LVLMS, which further exacerbates the *instruction-dependence* of the fine-tuned model. In summary, the limited ability of fine-tuned Qwen2.5-VL-3B and MedGemma-4B to generalize across diverse instructions leads to a significant degradation in multiple-choice VQA performance.

Overall, InstFree achieves the highest accuracy across all datasets among the LVLMS compared, demonstrating the superiority of the momentum proxy instruction. In addition, employing response shuffling (i.e., InstFree *w/* RS) further improves the average accuracy to 69.5%, demonstrating the effectiveness of the response shuffling. Although it shows a decrease in accuracy on WBCAtt compared to InstFree, the advantages of our response shuffling are demonstrated in attribute-wise accuracy. Fig. 5(a) and Fig. 5(b) show radar charts for each attribute on the WBCAtt and CBIS datasets, respectively. While leveraging inter-attribute correlations can improve overall accuracy, over-reliance on them may compromise the reliability of certain attribute predictions. Specifically, the WBCAtt dataset is susceptible to misclassification since some labels can be inferred from earlier parts of a response [26]. In this context, the superior accuracy achieved by response shuffling for primary targets that have strong correlations (e.g., label) highlights the effectiveness of the proposed method in reducing over-reliance on previous words. Similarly, applying response shuffling improves the overall accuracy on both the CBIS and SKINCON datasets, demonstrating our method’s effectiveness in enhancing the reliability of each attribute prediction across datasets.

2) *Comparison with Instruction-Free Tuning Variants*: We compared our method with two instruction-free tuning vari-

TABLE I: Multiple-choice VQA accuracy on the SKINCON, WBCAtt, and CBIS datasets. We compared our method (InstFree) with BLIP-2 [32], MedGemma-4B [3], PubMedVision-7B [4], Qwen2.5-VL-3B [17], and LLaMA-3.2-11B-Vision [16]. FT denotes fine-tuning, and RS denotes response shuffling. **Bold** indicates the highest accuracy, and underline denotes the second highest.

Model	SKINCON	WBCAtt	CBIS	Avg.
BLIP-2 (w/o FT)	8.7	35.2	4.6	16.1
MedGemma-4B (w/o FT)	14.3	37.3	39.2	30.2
PubMedVision-7B (w/o FT)	47.0	36.3	40.6	41.3
Qwen2.5-VL-3B (w/o FT)	37.7	32.8	36.0	35.5
LLaMA-3.2-11B-Vision (w/o FT)	39.9	34.6	43.0	39.1
MedGemma-4B (FT)	8.9 ± 1.76	45.9 ± 1.18	42.5 ± 2.23	32.4
Qwen2.5-VL-3B (FT)	42.0 ± 0.42	39.4 ± 0.19	39.3 ± 0.12	40.2
LLaMA-3.2-11B-Vision (FT)	59.4 ± 3.85	61.7 ± 3.72	63.9 ± 0.3	61.6
InstFree	69.8 ± 0.75	68.4 ± 0.61	65.0 ± 0.37	67.7
InstFree w/ RS	75.2 ± 0.9	<u>65.2 ± 1.39</u>	68.3 ± 0.37	69.5

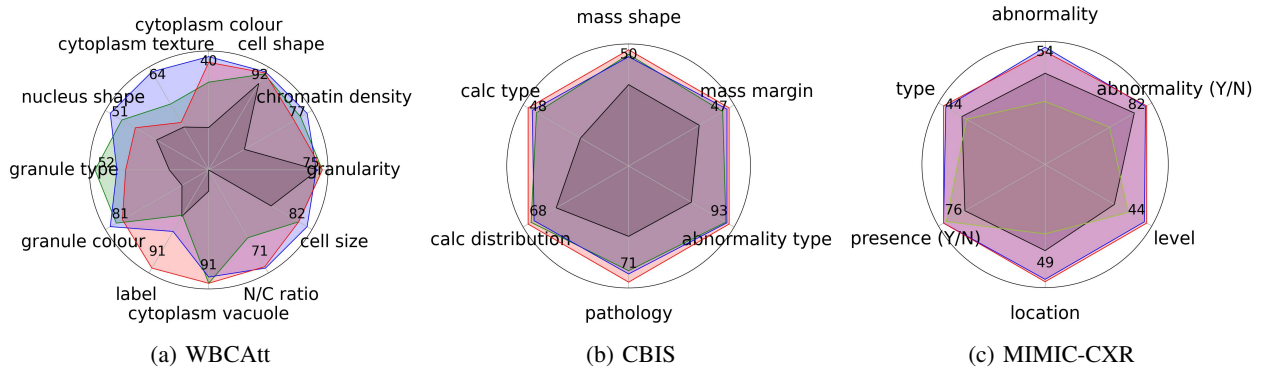


Fig. 5: Radar charts of the accuracy for each attribute (or question type) across the (a) WBCAtt, (b) CBIS, and (c) MIMIC-CXR datasets. LLaMA-3.2-11B-Vision (w/o FT) is shown in black, LLaMA-3.2-11B-Vision (FT) in green, InstFree in blue, InstFree w/ RS in red, and MedGemma-4B in yellow-green.

TABLE II: Multiple-choice VQA accuracy of instruction-free tuning variants on the SKINCON, WBCAtt, and CBIS datasets. Fix and Update denote models fine-tuned with fixed and continuously updating proxy instructions, respectively.

Method	SKINCON	WBCAtt	CBIS	Avg.
Fix	63.9 ± 1.52	65.1 ± 0.97	61.7 ± 1.49	63.5
Update	66.4 ± 2.55	63.6 ± 0.83	63.7 ± 0.49	64.5
InstFree	69.8 ± 0.75	68.4 ± 0.61	65.0 ± 0.37	67.7

ants, i.e., Fix and Update, to demonstrate the effectiveness of the proposed momentum proxy instruction. Fix used a fixed proxy instruction derived from a prior warm-up stage and updated only the vision encoder during fine-tuning, whereas Update referred to fine-tuning in which both the proxy instruction and the vision encoder were updated via gradient descent.

Table II shows the multiple-choice VQA accuracy of instruction-free tuning variants. Among the variants, accuracy differs between the Fix and Update, as Fix achieves higher performance on WBCAtt, while Update shows higher accuracy on SKINCON and CBIS. The superior accuracy of WBCAtt with Fix might be due to the vision encoder having fewer changes during fine-tuning, probably because the cells are always centered, which leads to more consistent image features. Notably, employing the momentum proxy instruction outperforms Fix by more than 4%, confirming the benefits of capturing overall fine-tuning trends while prioritizing updates to the vision encoder parameters.

TABLE III: VQA accuracy on the MIMIC-CXR dataset. We compared our method with MedGemma-4B [3], an instruction-tuned model trained on the MIMIC-CXR dataset, and LLaMA-3.2-11B-Vision [16].

Model	Accuracy
LLaMA-3.2-11B-Vision (w/o FT)	46.9
MedGemma-4B	44.7
InstFree	58.9 ± 0.29
InstFree w/ RS	59.3 ± 0.12

B. Comparison with an Instruction Tuned Model

We evaluated our method against an instruction-tuned model on the MIMIC-CXR dataset, i.e., MedGemma-4B-it [3], to demonstrate the superiority of our approach over instruction-tuned baselines. MedGemma-4B was fine-tuned on the MIMIC-CXR dataset and showed strong performance in report generation and classification of five diseases: atelectasis, cardiomegaly, consolidation, edema, and pleural effusion. Also, we compared our method with an LLaMA-3.2-11B-Vision-Instruct [16] (without fine-tuning) to provide a lower bound on performance. Since reports in the MIMIC-CXR dataset consist of findings and impression sections, we perform response shuffling between these sections without using a separator.

Table III shows multiple-choice VQA accuracy on the MIMIC-CXR dataset (i.e., Medical-CXR-VQA [31]), and Fig. 5(c) presents a radar chart of the accuracy for each question

TABLE IV: Ablation study of response shuffling on the SKINCON (SKN.), WBCAtt (WBC.), and CBIS datasets. Bal denotes balanced sampling; RS (“ ”) and Rand denote models fine-tuned with an incorrect separator and randomized text instructions, respectively.

Method	SKN.	WBC.	CBIS	Avg.
InstFree w/ Bal	65.4	63.4	60.8	63.2
InstFree w/ RS (“ ”)	67.9	57.9	67.2	64.3
InstFree w/ RS	75.2	65.2	68.3	69.5
FT w/ RS	74.1	62.0	67.3	67.8
FT w/ Rand	3.1	27.5	27.9	19.5

type. MedGemma-4B achieves high accuracy on presence-type questions, while exhibiting lower accuracy on other question types. We believe that the low accuracy across most MIMIC-CXR question types is due to limited exposure to diverse instructions during MedGemma-4B’s training. By contrast, presence-type questions beginning with “Is there” align closely with MedGemma-4B’s chest X-ray classification prompts and consequently yield higher accuracy. Moreover, the low accuracy on abnormality-type questions likely stems from the much larger pool of 281 answer candidates in MIMIC-CXR, compared with the five diseases considered in the MedGemma-4B evaluation. These observations suggest that discrepancies between training and evaluation instructions can significantly impact model performance, highlighting the challenges and limitations of constructing an instruction dataset that covers the full range of medical problems. Overall, InstFree and InstFree w/ RS achieve higher accuracy than MedGemma-4B across all question types. Given the difficulty of constructing instruction datasets that cover all question types, our approach provides a practical solution for developing an LVLM tailored to the target dataset.

C. Ablation Studies

1) *Ablation on Response Shuffling*: We conducted ablation studies on response shuffling using the SKINCON, WBCAtt, and CBIS datasets. First, we compared InstFree w/ Bal (balanced sampling) to investigate whether the issue originates from the model overfitting to previous word correlations or recurring response patterns. We calculate the frequency of each word and assign higher selection probabilities to samples that contain words with lower overall frequencies. Second, we compared InstFree w/ RS (“ ”) to demonstrate that accuracy degrades when response shuffling uses incorrect separators such as “ ” (instead of the “,” separator). Third, we compared FT w/ RS to show that response shuffling can improve VQA accuracy even when LLaMA-3.2-11B-Vision is fine-tuned with a text instruction. Lastly, we compared FT w/ Rand (fine-tuning LLaMA-3.2-11B-Vision with randomized text instructions) to demonstrate that diversifying instructions does not lead to better performance (as an extension of response shuffling). To do this, we randomly select an instruction from a set of 58 predefined text instructions, such as “Please report this medical scan.”.

Table IV shows the accuracy of the ablation study on response shuffling across the SKINCON, WBCAtt, and CBIS datasets. InstFree w/ Bal shows lower accuracy compared to

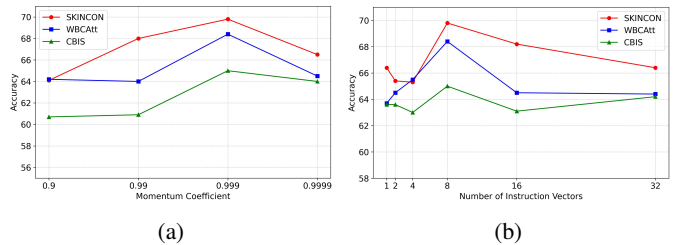


Fig. 6: Ablation study of (a) the momentum coefficient α and (b) the number of instruction vectors N on the SKINCON, WBCAtt, and CBIS datasets.

the model without balanced sampling, i.e., InstFree. These results indicate that oversampling of specific samples leads to overfitting and results in lower accuracy, suggesting that reducing over-reliance on previous words is more important. InstFree w/ RS (“ ”) shows lower accuracy than the model that uses a comma “,” as the separator. Although standard sentence segmentation libraries are generally sufficient, domain-specific datasets often contain text with poorly structured sentences; therefore, carefully designing strategies to separate elements is necessary for effective response shuffling. While FT w/ RS shows higher accuracy than the model without response shuffling, its accuracy remains lower than that of InstFree w/ RS, highlighting the benefits of the momentum proxy instruction. Meanwhile, FT w/ Rand exhibits significantly lower accuracy. This suggests that the fine-tuned model tends to ignore the given instructions, consistently generating responses that follow the format of our medical reports (i.e., *image-dependence*), such as “*plaque, scale...*” This result implies that diversifying instructions during fine-tuning degrades the LVLM’s instruction-following capability, thereby leading the model to generate responses primarily based on the visual input.

2) *Discussion of Misalignment*: As shown in Table IV (FT w/ Rand), fine-tuning the model to generate consistent responses across a broad range of instructions leads to a significant degradation of its pre-trained instruction-following capability. This degradation appears to stem from a misalignment between the fine-tuning dataset and the pre-training data, as the pre-training paired outputs vary in format depending on the instruction. Similarly, both the drift from the fixed proxy instruction during fine-tuning (see Fix in Table II) and the misalignment between a naively paired single instruction and the pre-training dataset (see FT in Table I) can be interpreted as factors that adversely affect instruction-following capability. Meanwhile, continuously minimizing misalignment during fine-tuning may appear ideal; however, excessive reliance on instructions (which will be discarded) through direct gradient descent can ultimately lead to a degradation in VQA performance (see Update in Table II). Within this context of misalignment, since most publicly available LVLMs do not release their datasets, manually replicating such datasets to reduce misalignment is impractical. Therefore, momentum proxy instruction offers a practical solution for fine-tuning LVLMs without instructions.

3) *Ablation on Coefficients and Instruction Scale*: We conducted ablation studies on the momentum proxy instruction using the SKINCON, WBCAtt, and CBIS datasets by varying the momentum coefficient and the number of instruction vectors to identify optimal hyperparameters. For the momentum coefficient α , we experimented with values of 0.9, 0.99, 0.999, and 0.9999, while setting the number of instruction vectors N to 8. For the number of instruction vectors N , we experimented with values of 1, 2, 4, 8, 16, and 32, while setting the momentum coefficient α to 0.999.

Fig. 6(a) shows the accuracy of the ablation study on the momentum coefficient. The value 0.999 yielded the highest accuracy, indicating that excessively fast or slow adaptation may limit performance improvements, similar to [23]. Fig. 6(b) shows the accuracy of the ablation study on the number of instruction vectors. The highest accuracy was achieved with 8 instruction vectors, whereas increasing the number to 32 resulted in lower performance. This may be related to general questions averaging about 8 tokens in length.

D. Qualitative VQA Analysis

Fig. 7 presents VQA results of LLaMA-3.2-11B-Vision on the WBCAtt dataset. In the case of descriptive instruction (a), the model without fine-tuning (*w/o* FT) identifies the image as a neutrophil, whereas fine-tuned models identify it as a monocyte, demonstrating that fine-tuning allows the model to identify images more precisely. InstFree and InstFree *w/* RS generate correct and natural text responses, whereas FT generates responses in the format of our medical reports. This suggests that using text instructions similar to those employed during fine-tuning may lead to overfitting (e.g., fixed-format outputs) or data leakage, highlighting the advantages of using the momentum proxy instruction in terms of generation quality and safety. Furthermore, response shuffling results in inconsistent output ordering in FT *w/* RS, whereas InstFree *w/* RS generates natural responses, demonstrating the greater robustness of our approach to output variability.

In the case of attribute-related instruction (b), InstFree *w/* RS accurately identifies the cell type and generates responses based on the appropriate fine-tuned attributes, whereas *w/o* FT misclassifies it as a neutrophil and generates responses accordingly (e.g., dense and granular; the correct is frosted). Meanwhile, although the correct fine-tuned attributes are present in the response, FT fails to follow the instructions and generates responses that exhibit *image-dependence*. These results indicate that our method is highly sensitive to the given instructions and confirm its superior instruction-following capability.

For instruction (c), which requires medical knowledge of relevant attributes, all models generate natural and accurate responses, demonstrating that they retain their pre-trained knowledge even after fine-tuning.

In the case of challenging instruction (d), *w/o* FT identifies the cell as a neutrophil and implies dysplasia, whereas InstFree *w/* RS recognizes that the shape is commonly seen in monocytes and therefore does not imply dysplasia. Meanwhile, FT generates a response that does not follow the instruction, similar to (b). These results demonstrate that our approach enables

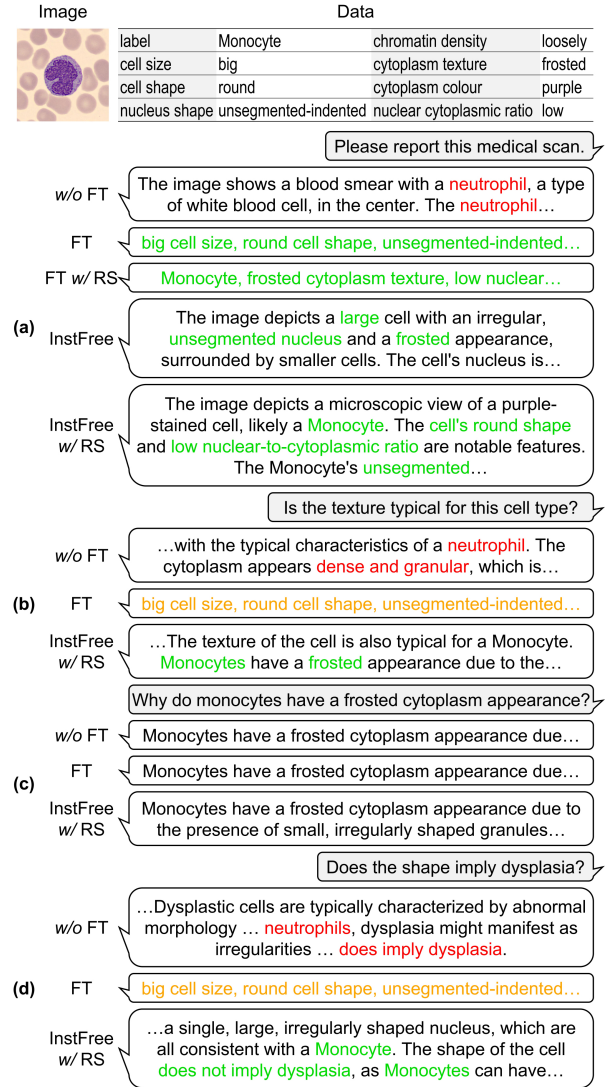


Fig. 7: Qualitative VQA results on the WBCAtt dataset. Correct responses are marked in green, incorrect responses are marked in red, and responses that do not follow instructions are marked in orange.

the model to respond flexibly to diverse instructions, without requiring expert-level human effort in dataset construction. In summary, the qualitative VQA analysis not only supports the quantitative success but also demonstrates the strengths of the proposed method beyond accuracy.

VI. CONCLUSION

We introduce an instruction-free tuning framework specifically tailored for the efficient fine-tuning of medical LVLMs. Our proposed momentum proxy instruction preserves the instruction-following capability of the pre-trained LVLm during fine-tuning, while simultaneously promoting updates to the visual encoder. This enables the fine-tuned model to flexibly respond to domain-specific instructions, even without explicit instructions during fine-tuning. Additionally, applying response shuffling during fine-tuning further mitigates the model's over-reliance on previous words, facilitating more

effective fine-tuning. Experimental results demonstrate that our method achieves superior accuracy across the SKINCON, WBCAtt, CBIS, and MIMIC-CXR datasets, significantly enhancing fine-tuning efficiency in medical domains.

- [1] C. Li, C. Wong, S. Zhang, N. Usuyama, H. Liu, J. Yang, T. Naumann, H. Poon, and J. Gao, "Llava-med: Training a large language-and-vision assistant for biomedicine in one day," *Advances in Neural Information Processing Systems*, vol. 36, pp. 28 541–28 564, 2023.
- [2] C. Zhou, P. Liu, P. Xu, S. Iyer, J. Sun, Y. Mao, X. Ma, A. Efrat, P. Yu, L. Yu *et al.*, "Lima: Less is more for alignment," *Advances in Neural Information Processing Systems*, vol. 36, pp. 55 006–55 021, 2023.
- [3] A. Sellergren, S. Kazemzadeh, T. Jaroensri, A. Kiraly, M. Traverse, T. Kohlberger, S. Xu, F. Jamil, C. Hughes, C. Lau *et al.*, "Medgemma technical report," *arXiv preprint arXiv:2507.05201*, 2025.
- [4] J. Chen, C. Gui, R. Ouyang, A. Gao, S. Chen, G. Chen, X. Wang, Z. Cai, K. Ji, X. Wan *et al.*, "Towards injecting medical visual knowledge into multimodal llms at scale," in *Proceedings of the 2024 Conference on Empirical Methods in Natural Language Processing*, 2024, pp. 7346–7370.
- [5] S. Moon, S. Pakhomov, N. Liu, J. O. Ryan, and G. B. Melton, "A sense inventory for clinical abbreviations and acronyms created using clinical notes and medical dictionary resources," *Journal of the American Medical Informatics Association*, vol. 21, no. 2, pp. 299–307, 2014.
- [6] R. Leaman, R. Khare, and Z. Lu, "Challenges in clinical natural language processing for automated disorder normalization," *Journal of biomedical informatics*, vol. 57, pp. 28–37, 2015.
- [7] C. E. Kahn Jr, C. P. Langlotz, E. S. Burnside, J. A. Carrino, D. S. Channin, D. M. Hovsepian, and D. L. Rubin, "Toward best practices in radiology reporting," *Radiology*, vol. 252, no. 3, pp. 852–856, 2009.
- [8] A. Favero, L. Zancato, M. Trager, S. Choudhary, P. Perera, A. Achille, A. Swaminathan, and S. Soatto, "Multi-modal hallucination control by visual information grounding," in *Proceedings of the IEEE/CVF Conference on Computer Vision and Pattern Recognition*, 2024, pp. 14 303–14 312.
- [9] S. Mishra, D. Khashabi, C. Baral, and H. Hajishirzi, "Cross-task generalization via natural language crowdsourcing instructions," in *Proceedings of the 60th Annual Meeting of the Association for Computational Linguistics (Volume 1: Long Papers)*, 2022, pp. 3470–3487.
- [10] R. Taori, I. Gulrajani, T. Zhang, Y. Dubois, X. Li, C. Guestrin, P. Liang, and T. B. Hashimoto, "Alpaca: A strong, replicable instruction-following model," *Stanford Center for Research on Foundation Models*. <https://crfm.stanford.edu/2023/03/13/alpaca.html>, vol. 3, no. 6, p. 7, 2023.
- [11] H. Touvron, T. Lavril, G. Izacard, X. Martinet, M.-A. Lachaux, T. Lacroix, B. Rozière, N. Goyal, E. Hambro, F. Azhar *et al.*, "Llama: Open and efficient foundation language models," *arXiv preprint arXiv:2302.13971*, 2023.
- [12] J. Achiam, S. Adler, S. Agarwal, L. Ahmad, I. Akkaya, F. L. Aleman, D. Almeida, J. Altschmidt, S. Altman, S. Anadkat *et al.*, "Gpt-4 technical report," *arXiv preprint arXiv:2303.08774*, 2023.
- [13] Y. Wang, Y. Kordi, S. Mishra, A. Liu, N. A. Smith, D. Khashabi, and H. Hajishirzi, "Self-instruct: Aligning language models with self-generated instructions," in *Proceedings of the 61st Annual Meeting of the Association for Computational Linguistics (Volume 1: Long Papers)*, 2023, pp. 13 484–13 508.
- [14] H. Liu, C. Li, Q. Wu, and Y. J. Lee, "Visual instruction tuning," *Advances in neural information processing systems*, vol. 36, pp. 34 892–34 916, 2023.
- [15] A. Radford, J. W. Kim, C. Hallacy, A. Ramesh, G. Goh, S. Agarwal, G. Sastry, A. Askell, P. Mishkin, J. Clark *et al.*, "Learning transferable visual models from natural language supervision," in *International conference on machine learning*. Pmlr, 2021, pp. 8748–8763.
- [16] A. Dubey, A. Jauhri, A. Pandey, A. Kadian, A. Al-Dahle, A. Letman, A. Mathur, A. Schelten, A. Yang, A. Fan *et al.*, "The llama 3 herd of models," *arXiv preprint arXiv:2407.21783*, 2024.
- [17] S. Bai, K. Chen, X. Liu, J. Wang, W. Ge, S. Song, K. Dang, P. Wang, S. Wang, J. Tang *et al.*, "Qwen2.5-vl technical report," *arXiv preprint arXiv:2502.13923*, 2025.
- [18] Z. Liu, K. Zhou, X. Zhao, D. Gao, Y. Li, and J.-R. Wen, "Vift: Towards visual instruction-free fine-tuning for large vision-language models," in *Findings of the Association for Computational Linguistics: EMNLP 2025*, 2025, pp. 10 341–10 366.
- [19] A. Dosovitskiy, L. Beyer, A. Kolesnikov, D. Weissenborn, X. Zhai, T. Unterthiner, M. Dehghani, M. Minderer, G. Heigold, S. Gelly, J. Uszkoreit, and N. Houlsby, "An image is worth 16x16 words: Transformers for image recognition at scale," in *International Conference on Learning Representations*, 2021.
- [20] J.-B. Alayrac, J. Donahue, P. Luc, A. Miech, I. Barr, Y. Hasson, K. Lenc, A. Mensch, K. Millican, M. Reynolds *et al.*, "Flamingo: a visual language model for few-shot learning," *Advances in neural information processing systems*, vol. 35, pp. 23 716–23 736, 2022.
- [21] torchtune, "torchtune: Pytorch's finetuning library," <https://github.com/pytorch/torchtune>, 2024.
- [22] X. L. Li and P. Liang, "Prefix-tuning: Optimizing continuous prompts for generation," in *Proceedings of the 59th Annual Meeting of the Association for Computational Linguistics and the 11th International Joint Conference on Natural Language Processing (Volume 1: Long Papers)*, 2021, pp. 4582–4597.
- [23] K. He, H. Fan, Y. Wu, S. Xie, and R. Girshick, "Momentum contrast for unsupervised visual representation learning," in *Proceedings of the IEEE/CVF conference on computer vision and pattern recognition*, 2020, pp. 9729–9738.
- [24] R. Daneshjou, M. Yuksekgonul, Z. R. Cai, R. Novoa, and J. Y. Zou, "Skincon: A skin disease dataset densely annotated by domain experts for fine-grained debugging and analysis," *Advances in Neural Information Processing Systems*, vol. 35, pp. 18 157–18 167, 2022.
- [25] M. Groh, C. Harris, L. Soenksen, F. Lau, R. Han, A. Kim, A. Koochek, and O. Badri, "Evaluating deep neural networks trained on clinical images in dermatology with the fitzpatrick 17k dataset," in *Proceedings of the IEEE/CVF conference on computer vision and pattern recognition*, 2021, pp. 1820–1828.
- [26] S. Tsutsui, W. Pang, and B. Wen, "Wbcatt: A white blood cell dataset annotated with detailed morphological attributes," *Advances in Neural Information Processing Systems*, vol. 36, pp. 50 796–50 824, 2023.
- [27] R. S. Lee, F. Gimenez, A. Hoogi, K. K. Miyake, M. Gorovoy, and D. L. Rubin, "A curated mammography data set for use in computer-aided detection and diagnosis research," *Scientific data*, vol. 4, no. 1, pp. 1–9, 2017.
- [28] A. E. Johnson, T. J. Pollard, S. J. Berkowitz, N. R. Greenbaum, M. P. Lungren, C.-y. Deng, R. G. Mark, and S. Horng, "Mimic-cxr, a de-identified publicly available database of chest radiographs with free-text reports," *Scientific data*, vol. 6, no. 1, p. 317, 2019.
- [29] J. M. Zambrano Chaves, S.-C. Huang, Y. Xu, H. Xu, N. Usuyama, S. Zhang, F. Wang, Y. Xie, M. Khademi, Z. Yang *et al.*, "A clinically accessible small multimodal radiology model and evaluation metric for chest x-ray findings," *Nature Communications*, vol. 16, no. 1, p. 3108, 2025.
- [30] N. Gaggion, C. Mosquera, L. Mansilla, J. M. Saidman, M. Aineseder, D. H. Milone, and E. Ferrante, "Chexmask: a large-scale dataset of anatomical segmentation masks for multi-center chest x-ray images," *Scientific Data*, vol. 11, no. 1, p. 511, 2024.
- [31] X. Hu, L. Gu, K. Kobayashi, L. Liu, M. Zhang, T. Harada, R. M. Summers, and Y. Zhu, "Interprettable medical image visual question answering via multi-modal relationship graph learning," *Medical Image Analysis*, vol. 97, p. 103279, 2024.
- [32] J. Li, D. Li, S. Savarese, and S. Hoi, "Blip-2: Bootstrapping language-image pre-training with frozen image encoders and large language models," in *International conference on machine learning*. PMLR, 2023, pp. 19 730–19 742.
- [33] S. Goyal, C. Baek, J. Z. Kolter, and A. Raghunathan, "Context-parametric inversion: Why instruction finetuning may not actually improve context reliance," in *The Thirteenth International Conference on Learning Representations*, 2025.